Euro. Jnl of Applied Mathematics (1997), *vol.* 8, *pp.* 485–505. Printed in the United Kingdom

© 1997 Cambridge University Press

The light fluid loading limit for fluid/solid interactions

R. V. CRASTER

Department of Theoretical Mechanics, University of Nottingham, Nottingham NG7 2RD, UK

(*Received 29 February 1996; revised 8 January 1997*)

Many elastodynamic solutions exist for wave interactions with defects upon or within an elastic half space bounded above by a vacuum. The aim of this paper is to significantly widen the scope of these solutions by showing that they can be directly utilized, when the vacuum is replaced by a fluid, to find the leading order acoustic (or elastic) responses in the light fluid-loading limit. Using the procedure developed here one can take virtually any elastodynamic solution and use it to generate the leading-order solution for a fluid-loaded elastic solid.

1 Introduction

Many applications involve fluid/solid wave interactions. These include structural acoustics, the acoustic microscope and wave interactions in geophysics. In these applications considerable effort has been taken to solve, asymptotically, heuristically, or otherwise, various model problems involving the reflection or generation of waves from a plane surface or inhomogeneities upon such a surface; for a line source in the fluid interacting with a plane fluid–solid interface, the wave structure is described in Tew (1992b). The dominant responses in the solid are longitudinal and shear cylindrical body waves together with a leaky Rayleigh wave that decays exponentially with distance from the source of the waves. This leaky wave is identified unambiguously only in the light fluid loading limit where it is a perturbation of the Rayleigh wave that would propagate unattenuated along the surface of the elastic solid when in contact with a vacuum. In addition there is an interfacial Stoneley wave (commonly called a Schölte wave) that decays exponentially with depth in both the fluid and solid materials; in the light fluid loading limit the decay is rapid in the solid and weak in the fluid. The fluid also supports a compressional cylindrical body wave and an exponentially decaying surface wave induced by the leaky Rayleigh wave. There are also head waves in both the fluid and solid that decay faster than the cylindrical waves; these head waves are generated by the cylindrical waves as they are unable to satisfy the surface boundary conditions without this correction. If the wave speed of the fluid is less than the shear wave speed of the solid then the head waves generated by the acoustic cylindrical wave in the solid are evanescent. A schematic, (Figure 1) shows these wavefronts for the waves generated by a vibrating semi-infinite interfacial rigid strip.

Light fluid-loading corresponds to the ratio of the fluid impedance to solid impedance relative to compressional waves being small, $\epsilon = \rho_f k_a/\rho k_0$ (ρ_f, ρ are the fluid and solid densities and k_0, k_a are the wavenumbers associated with compressional waves in the fluid and solid), the aim is to take advantage of this small parameter. If this parameter is zero

https://doi.org/10.1017/S0956792597003239 Published online by Cambridge University Press

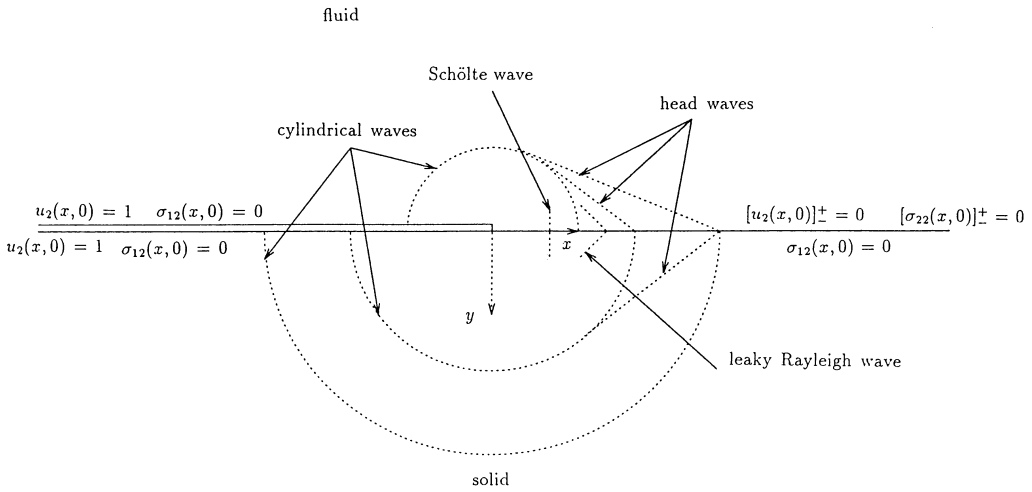


FIGURE 1. A schematic showing the radiated wavefronts for the waves generated by a vibrating semi-infinite interfacial rigid strip upon a fluid/solid interface with an $e^{-i\omega t}$ dependence suppressed.

the elastic half space is bounded above by a vacuum and the resulting mathematical problems are considerably simpler to solve. In essence these elastic solutions, derived in the absence of the fluid loading, are then used to drive the fluid response and this gives the leading order far field directivity associated with the cylindrical wave. This procedure is well-known in fluid–elastic plate problems; see, for instance, Crighton (1972), where a similar procedure is utilized; other related papers are Heckl (1962) and Maidanik (1967). In the fluid–elastic plate problems this approach is mainly useful for aerodynamic situations; for fluid–elastic solid interactions the range of utility is somewhat wider. This is because, not only is $\epsilon \ll 1$ in many cases, but the 'Mach' number relating the compressional wave speed of the fluid, say, water, to a typical Rayleigh wave speed is usually $O(1)$. Thus, by analogy with Crighton & Innes (1984), the fluid loading is light, even when the fluid is water.

It is important to note that the light fluid-loading limit is inherently non-uniform. A detailed study by Tew (1992a) identifies an underlying unattenuated beam structure that occurs along critical rays within the fluid for $1 \ll k_0 r \ll 1/\epsilon^2$ (similar behaviour occurs in the related fluid-loaded membrane or elastic plate problems, e.g. Crighton (1989)); the method used here evaluates these terms directly. In general, the acoustic directivity results shown as figures in the text are valid in the far field $k_0 r \gg 1/\epsilon^2$. This is not too severe a restriction when, as in the acoustic microscope, one may deal with ultrasonic frequencies of the order of GHz and for, say, aluminium–water the ratio of impedances is $\epsilon \sim 0.086$. To demonstrate that the procedure outlined here is useful for relatively large ϵ aluminium–water interfaces are taken for all the figures of typical directivity patterns.

The method presented here does not detect the presence of transition regions near a critical angle and the leading order behaviour of the unattenuated beam that forms in this intermediate region along that angle. Furthermore, a matching argument using Fresnel integrals can be used to determine the leading order behaviour of the interfacial Schölte waves.

The separation of fluid and solid responses allows problems to be solved that, for various

https://doi.org/10.1017/S0956792597003239 Published online by Cambridge University Press

reasons, cannot be solved explicitly and also allows a simpler physical interpretation of other problems sidestepping some complicated analysis. For instance along a fluid–solid interface a Rayleigh wave does not exist as a free surface wave – its replacement is an interfacial Stoneley wave (the Schölte wave) that typically has a wave speed much slower than the Rayleigh wave, for light fluid loading the Schölte wave travels at a speed marginally less than the compressional wave speed of the fluid. In the light fluid loading limit the Rayleigh wave becomes a leaky wave, some of its energy is now shed into the fluid and the wave exponentially decays with distance along the interface. In a practical situation the distances involved, and fluid coupling, may be small enough that this decay has little pronounced effect upon the Rayleigh wave. Nonetheless, it is awkward to mathematically consider, say, an incident leaky Rayleigh wave travelling towards a defect from infinity and then being scattered by the defect; the approach used here sidesteps this difficulty.

Other problems such as the scattering of an incident acoustic wave by a semi-infinite plate, coated with an acoustically soft material, lying along the interface lead to matrix Wiener–Hopf problems in a transform domain. It is not immediately apparent how one could factorize the resulting matrix explicitly so the problem appears unsolvable. Nonetheless the approach to be taken here will allow the far-field directives to be identified in the limit of light fluid-loading. For simplicity, a coated vibrating strip is considered; this is mathematically similar to the scattering problem for normal incidence. Furthermore it can be shown that this approach is equivalent to an asymptotic factorization of a matrix Wiener–Hopf problem.

Another useful aspect is that each problem is canonical and yields the far-field directivities for future use in conjunction with geometrical ray theory.

From a numerical point of view, many wave-defect interaction problems have been considered within an elastic half space. The addition of a coupling fluid leads to numerical complications thus it is of value to have an asymptotic method that generalizes the simpler elastic-vacuum problem in a direct manner.

The plan of the paper is to apply the procedure to two problems that have already been solved exactly to demonstrate the accuracy of the proposed scheme; the method is introduced on an intuitive basis. Then two other problems are solved: scattering of an incident Rayleigh wave by a semi-infinite rigid strip that lies along the interface, and the diffraction of an incident plane acoustic wave by a semi-infinite strip that is acoustically soft; in each case the far field directives are extracted. In addition, a numerical example is constructed and the approximate scattered directivity is compared with the exact solution. The aim of this paper is to demonstrate, in detail, that the perturbation scheme used here is accurate; in future work it will be used to tackle more complicated/realistic scattering problems.

2 Formulation

Consider a plane fluid–solid interface where the region $y > 0$ is an isotropic linear elastic material, and in $y < 0$ is a compressible fluid. The responses of the two half spaces are coupled together through either continuity or applied boundary conditions along $y = 0$. Time harmonic vibrations of frequency ω are considered. All physical variables are considered to have an $\mathrm{e}^{-i\omega t}$ time dependence, i.e. $u(x, y, t) = u(x, y)\,\mathrm{e}^{-i\omega t}$; this term is considered understood and suppressed henceforth.

https://doi.org/10.1017/S0956792597003239 Published online by Cambridge University Press

The elastic material in $y > 0$ has Lamé constants λ, μ and density ρ. The stresses, σ_{ij}, in the material are related to the displacements, u_i, via

$$\sigma_{ij} = \lambda \epsilon_{kk}\, \delta_{ij} + 2\mu \epsilon_{ij}, \quad \text{with} \quad \epsilon_{ij} = \tfrac{1}{2}(u_{i,j} + u_{j,i}). \tag{2.1}$$

A Cartesian coordinate system is adopted with x_1, x_2 corresponding to x, y. The governing equations in the elastic solid are $\sigma_{ij,j} = -\rho\omega^2 u_i$. Adopting displacement potentials ϕ and ψ, such that $\mathbf{u} = \nabla\phi + \nabla \times \psi \mathbf{e}_z$, that satisfy

$$\nabla^2 \phi + k_d^2 \phi = 0, \quad \nabla^2 \psi + k_s^2 \psi = 0, \tag{2.2}$$

simplifies the analysis slightly. The wavenumbers k_d, k_s are defined as

$$k_d^2 = \frac{\rho\omega^2}{(\lambda + 2\mu)}, \quad k_s^2 = \frac{\rho\omega^2}{\mu}, \tag{2.3}$$

and the corresponding wave speeds c_d, c_2 are given by $k_2 = \omega/c_s$, $k_d = \omega/c_d$. The subscripts s, d denote the variables associated with the shear and dilatational waves, respectively.

The compressible fluid in $y < 0$ is effectively an elastic material that supports no shear stresses, hence $\sigma_{ij} = \lambda_f \epsilon_{kk}\, \delta_{ij}$, the governing equations are the same as those for an elastic solid, and a potential χ is introduced so that $-i\omega u_i = (\nabla\chi)_{,i}$. This potential satisfies

$$\nabla^2 \chi + k_0^2 \chi = 0, \quad k_0^2 = \frac{\rho_f \omega^2}{\lambda_f}. \tag{2.4}$$

A coupling parameter ϵ occurs in the analysis; it is defined as $\epsilon = \rho_f k_d / \rho k_0$, and gives a measure of the fluid–solid coupling. The density of the fluid is defined as ρ_f. The situation when $\epsilon \ll 1$ is the light fluid-loading limit. It will be implicitly assumed that $k_0 > k_s (> k_d)$ here, that is, the shear wavespeed of the solid is greater than the compressional wavespeed of the fluid, this is usually the case; exceptions are combinations such as plastic/water interfaces.

Considerable use will be made of Fourier transforms defined as

$$F(\xi) = \int_{-\infty}^{\infty} f(x)\, \mathrm{e}^{i\xi x}\, \mathrm{d}x \quad \text{with inverse} \quad f(x) = \frac{1}{2\pi} \int_{\Gamma} F(\xi)\, \mathrm{e}^{-i\xi x}\, \mathrm{d}\xi, \tag{2.5}$$

where the path Γ runs along the real axis from $-\infty$ to ∞ and is indented so that it lies below any branch points and zeros that occur in the analysis along the positive real axis, and above those that occur along the negative axis. It is also useful to have the displacements and stresses in the transform domain: in $y > 0$ the material is elastic and the Fourier transformed displacements and stresses are

$$u_1(\xi, y) = -i\xi\, A(\xi)\, \mathrm{e}^{-\gamma_d(\xi) y} - \gamma_s(\xi)\, B(\xi)\, \mathrm{e}^{-\gamma_s(\xi) y}, \tag{2.6}$$

$$u_2(\xi, y) = -\gamma_d(\xi)\, A(\xi)\, \mathrm{e}^{-\gamma_d(\xi) y} + i\xi\, B(\xi)\, \mathrm{e}^{-\gamma_s(\xi) y}, \tag{2.7}$$

$$\sigma_{12}(\xi, y) = \mu(2i\xi\, \gamma_d(\xi)\, \mathrm{A}(\xi)\, \mathrm{e}^{-\gamma_d(\xi) y} + B(\xi)\, (\xi^2 + \gamma_s^2(\xi))\, \mathrm{e}^{-\gamma_s(\xi) y}), \tag{2.8}$$

$$\sigma_{22}(\xi, y) = \mu((2\xi^2 - k_s^2)\, A(\xi)\, \mathrm{e}^{-\gamma_d(\xi) y} - 2i\xi\, \gamma_s(\xi)\, B(\xi)\, \mathrm{e}^{-\gamma_s(\xi) y}). \tag{2.9}$$

https://doi.org/10.1017/S0956792597003239 Published online by Cambridge University Press

The functions $A(\xi)$, $B(\xi)$ are as yet unknown functions of ξ. In the fluid region $y < 0$ the relevant Fourier transformed variables are

$$-i\omega u_2(\xi, y) = \gamma_0(\xi)\, C(\xi)\, \mathrm{e}^{\gamma_0(\xi) y}, \quad \sigma_{22}(\xi, y) = -i\rho_f \omega C(\xi)\, \mathrm{e}^{\gamma_0(\xi) y}, \tag{2.10}$$

with $C(\xi)$ an unknown function of ξ.

The functions $\gamma_d(\xi)$, $\gamma_s(\xi)$ and $\gamma_0(\xi)$ that appear are defined as $\gamma_q(\xi) = (\xi^2 - k_q^2)^{\frac{1}{2}}$ with $q = d$, s or 0. The functions have branch points at $+k_q$, $-k_q$ that, when Γ is suitably indented, lie in the upper, lower half of the complex ξ plane, respectively. The branch cuts are taken from k_q to ∞ above the contour Γ and from $-k_q$ to $-\infty$ below Γ. The precise position of the branch cuts in each half plane is irrelevant at this stage of the analysis; the Riemann sheet chosen is such that $\gamma_q(0) = -ik_q$. As in most elastodynamic studies the Rayleigh function, $R(\xi)$, will occur naturally and is defined as

$$R(\xi) = (2\xi^2 - k_s^2)^2 - 4\xi^2 \gamma_s(\xi)\, \gamma_d(\xi); \tag{2.11}$$

this function has two real zeros at $\pm k_r$ where k_r is the wavenumber associated with the Rayleigh surface wave.

3 Comparison with known results

To demonstrate the method advocated here two problems are briefly reworked. The first is scattering by a surface inhomogeneity, in effect this is modelled as a jump in normal stress at the interface, this is treated in detail by Tew (1992a). The second is the vibration of a semi-infinite rigid strip in lubricated contact with the elastic solid, which is treated in detail in Craster (1996a). The analysis is performed in the transform domain.

For simplicity, the surface inhomogeneity is taken as an infinitesimally thin surface depression and the leading order effect of the defect is to consider it to be a line source on the surface of the elastic solid. This does not have any relationship to any specific defect geometry, but is used to investigate the type of wave structure that can be generated. If we ignore the fluid altogether and treat the elastic solid in isolation, that is we consider a traction free elastic half space with a line source loading, this is Lamb's problem for which the surface displacement is well known (see, for instance, Achenbach (1973)). This surface displacement is used to force the fluid response; that is we now ignore the solid, replacing it by a plane rigid boundary that has the surface displacement found from the elastic problem, hence the fluid initially sees a plane surface with a given displacement. From this we deduce that the fluid potential is approximately

$$\chi(x, y) = \frac{-i}{2\pi} \int_\Gamma \frac{k_s^4 F_0}{\omega\rho} \frac{\gamma_d(\xi)}{\gamma_0(\xi)\, R(\xi)} \mathrm{e}^{-i\xi x + \gamma_0(\xi) y}\, \mathrm{d}\xi, \tag{3.1}$$

where F_0 is the strength of the line source. The exact solution is the same as (3.1), but with $R(\xi)$ replaced by $R(\xi) + (\epsilon k_0 k_s^4 \gamma_d / k_d \gamma_0)$ so the separation of fluid and solid responses yields the leading order approximation of the full solution in the transform domain. Clearly the full solution contains a more complete analytical picture than the expansion; in particular the leaky Rayleigh pole and the pole corresponding to the Schölte wave are not described precisely by Eq. (3.1). Hence, one loses some of the analytical structure of the full problem; nonetheless, some details such as the far-field acoustic directivities and a representation for the leading order behaviour of the surface wave associated with the Rayleigh wave are

https://doi.org/10.1017/S0956792597003239 Published online by Cambridge University Press

captured accurately. The far-field cylindrical wave structure is extracted using the saddle point method and one obtains from Eq. (3.1) that

$$\chi(r,\theta) \sim \frac{k_s^4 F_0}{\omega\rho}\frac{\gamma_d(k_0\cos\theta)}{R(k_0\cos\theta)}\frac{\mathrm{e}^{ik_0 r-\frac{i\pi}{4}}}{(2\pi k_0 r)^{\frac{1}{2}}}, \tag{3.2}$$

for $k_0 r \gg 1$, where r, θ are polar coordinates centred upon the defect (note that $x = r\cos\theta$, $y = -r\sin\theta$); for comparative purposes, a typical directivity pattern shape, $|D(\theta)| = |\gamma_d(k_0\cos\theta)/R(k_0\cos\theta)|$, is shown for an aluminium-water interface (for which $\epsilon = 0.086$). In Figure 2 the dashed line corresponds to the approximate result and the solid line is exact. It is clear that the dominant responses, together with lesser peaks generated by interaction with shear and compressional waves in the solid, are also detected. The intense beam formation along the Rayleigh angles is clearly detected, as is the response due to the surface wave, although the approximation detects peaks of infinite size.

Similar accuracy is obtained for the directivities within the elastic solid, where to leading order they are the same as those for Lamb's problem.

One also obtains an expression for a surface wave in the fluid propagating with the Rayleigh wavespeed that is close to that found directly, i.e. for $x > 0$

$$\chi^R(x,y) \sim \frac{-k_s^4 F_0}{\omega\rho}\frac{\gamma_d(-k_r)}{\gamma_0(-k_r)\,R'(-k_r)}\mathrm{e}^{ik_r x+\gamma_0(-k_r)y}. \tag{3.3}$$

This is the same as the leading-order term for the leaky Rayleigh wave found from the full solution. In addition, from Eq. (3.1) it is clear that a non-uniformity occurs as the Rayleigh pole approaches the saddle point, crucially however the Rayleigh pole in Eq. (3.1) is real, and does not contain the imaginary part that the pole corresponding to the leaky Rayleigh wave, from the full expression, does. A transition solution valid in the neighbourhood of the Rayleigh angle $\theta_r = \cos^{-1} k_r/k_0$ is

$$\chi(r,\theta) = -\frac{k_s^4 F_0(k_r^2-k_d^2)^{\frac{1}{2}}\mathrm{e}^{ik_0 r+\frac{i\pi}{4}}}{\sqrt{\pi}\,\omega\rho(k_0^2-k_r^2)^{\frac{1}{2}}R'(-k_r)}\mathrm{e}^{i\eta^2}\int_\eta^\infty \mathrm{e}^{i\tau^2}\,\mathrm{d}\tau, \quad \eta = \epsilon\bar{\theta}(k_0 r)^{\frac{1}{2}}/\sqrt{2}, \tag{3.4}$$

where $\theta = \theta_r + \epsilon\bar{\theta}$ is the rescaling adopted. Crucially, this predicts that the influence of the Rayleigh surface wave extends into the fluid in a region $\theta < \theta_r$ and is cut-off at the Rayleigh angle. In addition, an unattenuated beam forms in an intermediate region $1 \ll k_0 r \ll 1/\epsilon^2$ where it has the form

$$\chi(r,\theta) = \frac{-ik_s^4 F_0(k_r^2-k_d^2)^{\frac{1}{2}}\mathrm{e}^{ik_0 r}}{\omega\rho(k_0^2-k_r^2)^{\frac{1}{2}}2R'(-k_r)}. \tag{3.5}$$

These are the leading-order solutions in ϵ, as comparison with the full solutions from Tew (1992a) shows.

There is an error in the approximation in the neighbourhood of the interface – clearly, the incorrect boundary conditions have been taken and the interfacial Schölte wave is not detected. This is corrected for by assuming the existence of an interfacial wave

$$\chi_{sch}(x,y) \sim \epsilon A\,\mathrm{e}^{ik_{sch}x+(k_{sch}^2-k_0^2)^{\frac{1}{2}}y} \tag{3.6}$$

that satisfies the continuity boundary conditions, and then using Fresnel integrals to match

https://doi.org/10.1017/S0956792597003239 Published online by Cambridge University Press

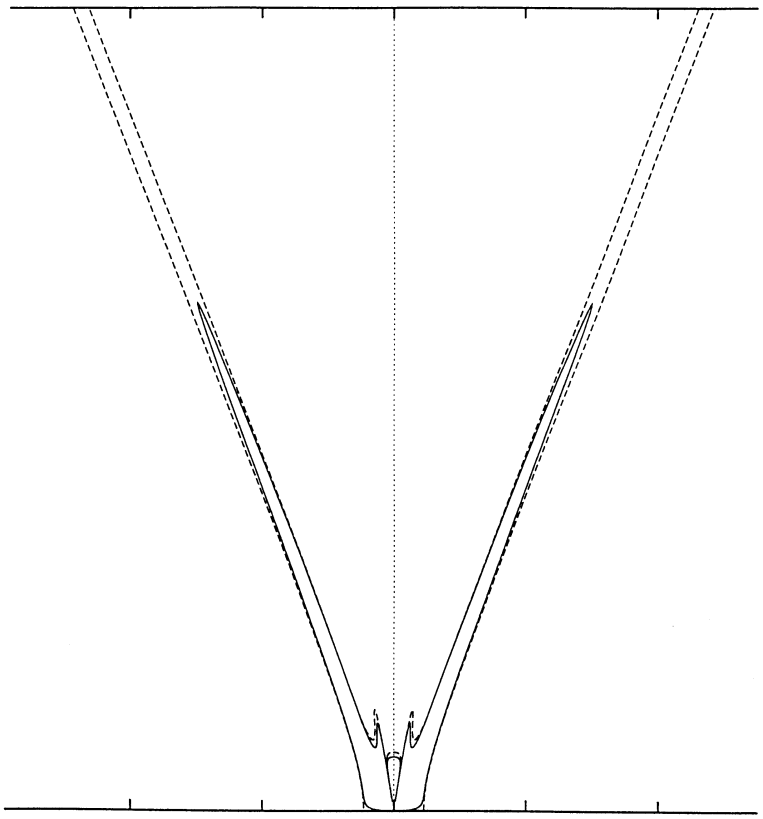


FIGURE 2. A typical directivity shape (for aluminium–water) for scattering by a surface line source, the dashed line is the approximate result and the solid line is exact.

this to the cylindrical wave as $\theta \sim \epsilon\bar{\theta}$ to determine A. This yields the leading order behaviour of the Schölte wave in the light fluid limit where expressions (5.9, 5.10) are required. A similar approach has recently been used by Barbone (1995) to identify the surface waves occurring in diffraction problems by impedance surfaces.

The main difference is that the full solutions have a corrected cut-off angle for the region of influence of the leaky Rayleigh wave that is $O(\epsilon)$ less than that found here. There are also transition regions found due to the Schölte waves that are not detected directly using the approximate approach, but a simple matching scheme determines these. All the crucial salient points are exposed using the approach outlined above. One can continue the iterative procedure, that is separating the fluid and solid responses, to obtain a direct expansion in powers of ϵ of the exact expression. The radiation damping of the peaks along the Rayleigh angle are not found using the procedure outlined above. However, one could displace the Rayleigh pole to its leaky Rayleigh position and then get improved results; the aim here has been to proceed as if we were unaware of the position of the leaky pole *a priori*.

Now consider a semi-infinite rigid strip that lies along the interface $y = 0$ for $x < 0$. The strip is taken to be in lubricated contact with the elastic solid and is acoustically hard. The first of these conditions is hard to physically realise, nonetheless, the results should be of practical significance as the effect of an abrupt change in boundary conditions can be

https://doi.org/10.1017/S0956792597003239 Published online by Cambridge University Press

evaluated; the full solution is in Craster (1996a). For simplicity, consider a vibrating strip for which the boundary conditions for the full problem, on $y = 0$, are

$$u_2(x,0) = 1 \quad \text{for} \quad x < 0 \quad \text{and} \quad [u_2(x,0)] = [\sigma_{22}(x,0)] = 0 \quad \text{for} \quad x > 0, \tag{3.7}$$

that is an applied displacement for $x < 0$ and continuity of surface traction and normal displacement along the common interface $x > 0$. The braces denote jumps in quantities across the interface. In addition, the lubricated contact condition and the absence of shear stresses in the fluid lead to an additional condition on $y = 0$ that $\sigma_{12}(x,0) = 0$.

To apply the approximate method we treat the elastic half-space firstly in isolation; initially, the fluid is effectively absent and one solves an elastic problem in $y > 0$ with the same boundary conditions as above, but with $\sigma_{22}(\xi,0) = 0$ on $y = 0$ for $x > 0$, which is a traction free interface. The solution is found in terms of half-range Fourier transforms

$$U_+(\xi) = \int_0^\infty u_2(x,0)\,\mathrm{e}^{i\xi x}\,\mathrm{d}x, \quad T_-(\xi) = \int_{-\infty}^0 \sigma_{22}(x,0)\,\mathrm{e}^{i\xi x}\,\mathrm{d}x. \tag{3.8}$$

The subscripts, $+$, $-$, denote functions that are analytic in the upper and lower halves of the complex ξ plane, respectively. These transforms together with the boundary conditions, and edge conditions that the displacements are non-singular at the edge of the strip, lead to the Wiener–Hopf functional equation

$$\frac{(\xi+k_r)\,S_+(\xi)}{(\xi+k_d)^{\frac{1}{2}}}\left(U_+(\xi)+\frac{1}{i\xi_-}\right) - \frac{S_+(0)\,k_r}{i\xi_-\,k_d^{\frac{1}{2}}} = \frac{k_s^2(\xi-k_d)^{\frac{1}{2}}\,T_-(\xi)}{(\xi-k_r)\,S_-(\xi)\,2\mu(k_d^2-k_s^2)} - \frac{S_+(0)\,k_r}{i\xi_-\,k_d^{\frac{1}{2}}} = 0, \tag{3.9}$$

the subscript on $1/i\xi_-$ denotes that the path Γ is taken to lie beneath this pole, and hence this function is analytic in the minus region. Equation (3.9) gives a non-zero surface displacement on $y = 0$ for $x > 0$ that is represented by the transform $U_+(\xi)$. The function $S(\xi) = R(\xi)/2(k_d^2-k_s^2)(\xi^2-k_r^2)$ and is split into a product of functions analytic in the upper and lower halves of the complex ξ plane, i.e. $S(\xi) = S_+(\xi)\,S_-(\xi)$ in Appendix A.

In so far as the fluid is concerned, it sees a plane surface with applied displacements given by the Fourier inverse of $U_+(\xi)$ for $x > 0$ and $u_2(x,0) = 1$ for $x < 0$, the resulting fluid potential is then found from the transform representation of $u_2(\xi,y)$ in (2.10) as

$$\frac{\chi(x,y)}{-i\omega} = \frac{1}{2\pi}\int_\Gamma \frac{S_+(0)\,k_r(\xi+k_d)^{\frac{1}{2}}\,\mathrm{e}^{-i\xi x+\gamma_0(\xi)y}\,\mathrm{d}\xi}{i\xi_-k_d^{\frac{1}{2}}\,S_+(\xi)\,(\xi+k_r)\,\gamma_0(\xi)}. \tag{3.10}$$

This compares with the full solution that, from Craster (1996a), is

$$\frac{\chi(x,y)}{-i\omega} = \frac{1}{2\pi}\int_\Gamma \frac{L_+(0)\,k_{sch}(\xi+k_d)^{\frac{1}{2}}\,\mathrm{e}^{-i\xi x+\gamma_0(\xi)y}\,\mathrm{d}\xi}{i\xi_-\,k_d^{\frac{1}{2}}\,L_+(\xi)\,(\xi+k_{sch})\,\gamma_0(\xi)}. \tag{3.11}$$

The function $L(\xi)$ is a function that is similar to $S(\xi)$ defined above, but with an extra term involving ϵ; it is $L(\xi) = (R(\xi)+(\epsilon k_0\,k_s^4\,\gamma_d/k_d\,\gamma_0))/2(k_d^2-k_s^2)(\xi^2-k_{sch}^2)$. Crucially, the numerator of this function has a real zero, at k_{sch}, that gives rise to the interfacial Schölte wave, that for small ϵ, is close to the branch point at k_0; this is not close to the Rayleigh pole k_r that appears in $S(\xi)$. At first sight, the appearance of these zeros that are not related (or even close, when ϵ is small) explicitly in the above formulae might suggest that the approximation is ill-founded. However, we are really factorising just the numerators of

https://doi.org/10.1017/S0956792597003239 Published online by Cambridge University Press

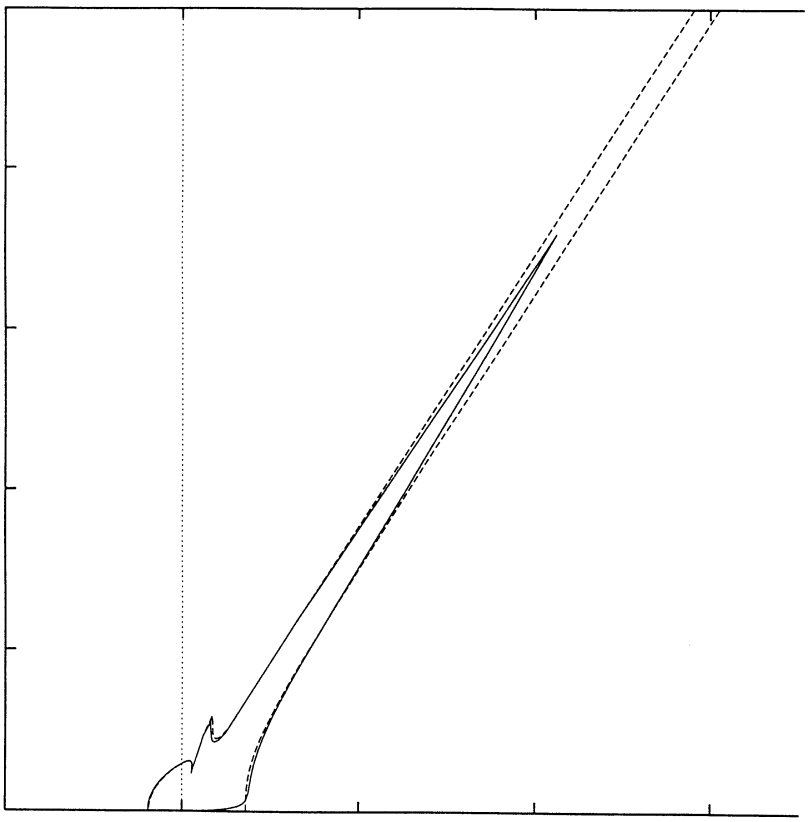


FIGURE 3. A typical directivity shape (for aluminium–water) for a vibrating semi-infinite rigid strip, the dashed line is the approximate result and the solid line is exact.

$L(\xi)$, $S(\xi)$ (these are the same apart from the term involving ϵ); the zeros are introduced as a mathematical device to aid the factorisations of these functions.

In both cases, a plane compressional wave is identified from the simple pole at zero together with a far field cylindrical wave in the fluid that is, from Eq. (3.10) and using the saddle point approach, found as

$$\chi(r,\theta) = \frac{i\omega}{(2\pi k_0 r)^{\frac{1}{2}} k_0 \cos\theta\, k_d^{\frac{1}{2}} S_-(k_0\cos\theta)\,(k_r - k_0\cos\theta)} \frac{k_r S_+(0)\,(k_d - k_0\cos\theta)^{\frac{1}{2}}}{} \mathrm{e}^{ik_0 r - \frac{i\pi}{4}} \tag{3.12}$$

and a similar formula with k_{sch} replacing k_r and $L(\xi)$ replacing $S(\xi)$ is found for the full problem. The polar coordinates r and θ are centred upon the plate edge, $0 < \theta < \pi$ and $\theta = 0$ corresponds to $y = 0,\ x > 0$. The field is written as $\chi(r,\theta)/(-i\omega) = D(\theta)\,(k_0 r)^{-\frac{1}{2}}$ $\mathrm{e}^{ik_0 r - \frac{i\pi}{4}}$; a typical directivity pattern shape is shown for $|\cos\theta\, D(\theta)|$, for an aluminium–water interface in Figure 3, where the solid line corresponds to the exact result and dashed line is approximate. The $\cos\theta$ term is used to remove the non-uniformity introduced at $\theta = \pi/2$ by the variation as one approaches the cut-off region associated with the plane compressional wave. There are also surface Schölte and leaky Rayleigh waves generated together with body waves in the solid. A similar accuracy is obtained for the directivities associated with the shear and dilatational waves within the elastic solid that to leading-

https://doi.org/10.1017/S0956792597003239 Published online by Cambridge University Press

order are just the usual elastic result and for the Rayleigh/leaky Rayleigh surface waves outside their non-uniform region, that is $k_0 x \gg 1/\epsilon^2$. As the Rayleigh pole and saddle point approach each other a transition solution is required in the neighbourhood of the Rayleigh angle θ_r. This correctly identifies the leading order behaviour of an unattenuated beam structure in an intermediate region.

To determine the Schölte wave we assume the existence of this interfacial wave in a region close to the interface; this ensures the continuity boundary conditions are satisfied, as

$$\chi_{sch}(x, y) \sim \epsilon A \, \mathrm{e}^{ik_{sch}x + (k_{sch}^2 - k_0^2)^{\frac{1}{2}} y}; \tag{3.13}$$

by using (5.9, 5.10) this becomes

$$\chi(\bar{r}, \bar{\theta}) \sim A\epsilon \, \mathrm{e}^{\frac{ik_0 \bar{r}}{\epsilon^2}((1 - \frac{1}{2}\epsilon^2(\bar{\theta} - iu)^2)} \tag{3.14}$$

in polar coordinates; $\bar{r} = \epsilon^2 r$ and $\epsilon\bar{\theta} = \theta$ is the appropriate scaling along the interface and the constant u is defined in Eq. (5.10). One then chooses the potential to be in the form

$$\chi(\bar{r}, \bar{\theta}) \sim B \, \mathrm{e}^{ik_0 r - \frac{i\pi}{4}} (F((k_0 \bar{r}/2)^{\frac{1}{2}}(\bar{\theta} - iu)) - F((k_0 \bar{r}/2)^{\frac{1}{2}}(\bar{\theta} + iu))). \tag{3.15}$$

A and B are constants to be found, and the $F(\eta)$ are Fresnel integrals defined as

$$F(\eta) = \mathrm{e}^{i\eta^2} \int_{\eta}^{\infty} \mathrm{e}^{i\tau^2} \, \mathrm{d}\tau.$$

In the limit when $\bar{\theta} > u$ and $k_0 \bar{r} \gg 1$ cylindrical wave solutions are recovered that can be matched to (3.12) to determine B. In $\bar{\theta} < u$ the Fresnel integrals give a term of the form (3.14), hence relating A to B. To leading order, this constant can be shown to be the same as that found in Craster (1996a) directly.

To summarise: the approximate method identifies far-field directivities valid for $k_0 r \gg 1/\epsilon^2$ and $k_{s,d} r \gg 1$. It also identifies a surface Rayleigh wave that contains no exponential decay with distance along the interface. The unattenuated beam formation in an intermediate region along the Rayleigh angle is also found. The existence of the interfacial Schölte wave is not directly identified, but a simple matching scheme that assumes its existence can be used to find the leading order amplitude of the wave. The simplicity of the approach and the accuracy of the far-field directivity, and results associated with the Rayleigh wave and transition regions along the Rayleigh angle, suggest that this is worth pursuing, particularly given the complexity of some full interfacial problems versus their elastodynamic counterparts.

4 An acoustically soft strip

The samples above are relatively simple, in so far as they are formally solved exactly, but it is not hard to find examples that are non-trivial, and for which it is not immediately apparent how a formal solution could be obtained. If the rigid strip considered above was a thin elastic plate, with different material properties to the elastic solid, the resulting analysis is formidable. A simpler problem that demonstrates the analytical problems is the extreme case of a rigid strip coated with a perfectly absorbing boundary on the side facing

https://doi.org/10.1017/S0956792597003239 Published online by Cambridge University Press

the fluid, that is, an acoustically soft strip. Similar problems involving fluid loaded membranes or elastic plates have been considered by Rawlins (1975) and Abrahams (1985). In practical terms this provides a model for the sound disturbance created by a vibrating panel that is coated with an absorbing layer; a similar analysis follows for the diffraction of incoming plane waves.

The boundary conditions on $y = 0$ for $x > 0$ are the same as in Eq. (3.7) above; the zero shear stress condition will also be assumed. However, on the plate,

$$\sigma_{22}(x, 0^-) = 0, \quad u_2(x, 0^+) = 1 \quad \text{for} \quad x < 0. \tag{4.1}$$

The superscripts $+$, $-$ are used to denote the limit as $y \to 0^{\pm}$. Separating the fluid and solid responses once more, the leading order elastic solution is given by (3.9) again. The only change is to the calculations involving the fluid where now we have $u_2(x, 0)$ given by the inverse transform of $U_+(\xi)$ from (3.9) for $x > 0$ once more, but the condition on $x < 0$ becomes $\sigma_{22}(x, 0) = 0$. A Wiener–Hopf analysis leads to

$$\frac{U_-(\xi)}{\gamma_0(\xi)} + \left(\frac{U_+}{\gamma_{0-}}\right)_l(\xi) = \frac{-\gamma_{0+}(\xi)\,\sigma_+(\xi)}{\rho_f \omega^2} - \frac{U_+(\xi)}{\gamma_{0-}(\xi)} + \left(\frac{U_+}{\gamma_{0-}}\right)_l(\xi) = 0, \tag{4.2}$$

where $\sigma_+(\xi)$, $U_-(\xi)$ are the half range transforms of the unknown normal stress along the interface and the normal displacement along the plate, both evaluated as $y \to 0^-$, and $\gamma_{0\pm}(\xi)$ are the multiplicative splits of the function $\gamma_0(\xi)$, that is, $\gamma_0(\xi) = \gamma_{0-}(\xi)\,\gamma_{0+}(\xi) = (\xi - k_0)^{\frac{1}{2}}(\xi + k_0)^{\frac{1}{2}}$. The subscript l denotes a function analytic in the lower half of the complex ξ plane that is deduced via an additive split, that is, $F(\xi) = F_u(\xi) + F_l(\xi)$ say, where u similarly denotes a function analytic in the upper plane. Hence,

$$\left(\frac{U_+}{\gamma_{0-}}\right)_l(\xi) = \frac{-1}{2\pi i}\int_\Gamma \frac{U_+(z)}{\gamma_{0-}(z)}\frac{dz}{(z-\xi)} \tag{4.3}$$

which has the behaviour that it tends to zero as $|\xi| \to \infty$ and ξ lies below the path of integration. An explicit representation is

$$\left(\frac{U_+}{\gamma_{0-}}\right)_l(\xi) = \frac{1}{\pi}\int_{k_0}^{\infty}\left(\frac{k_r\,S_+(0)\,(\tau + k_d)^{\frac{1}{2}}}{k_d^{\frac{1}{2}}(\tau + k_r)\,S_+(\tau)} - 1\right)\frac{d\tau}{\tau(\tau - k_0)^{\frac{1}{2}}(\tau - \xi)}. \tag{4.4}$$

From this, one finds the fluid potential as

$$\chi(x, y) = \frac{1}{2\pi}\int_\Gamma \frac{-i\omega}{\gamma_{0+}(\xi)}\left(\frac{U_+(\xi)}{\gamma_{0-}(\xi)}\right) - \left(\frac{U_+}{\gamma_{0-}}\right)_l(\xi)\Big)\mathrm{e}^{-i\xi x + \gamma_0(\xi) y}\,\mathrm{d}\xi. \tag{4.5}$$

The far-field directivity is deduced using the saddle point method once more, and it is compared to the hard strip case in figure 4. Specifically, this is a typical directivity pattern for $|D(\theta)\cos\theta|$ for aluminium-water. The main features of this diffracted cylindrical wave are effectively unchanged with both situations showing beam formation along the Rayleigh angle. Although there are fundamental differences in the responses of the other waves, most importantly there is, of course, no longer a compressional plane wave within the fluid.

https://doi.org/10.1017/S0956792597003239 Published online by Cambridge University Press

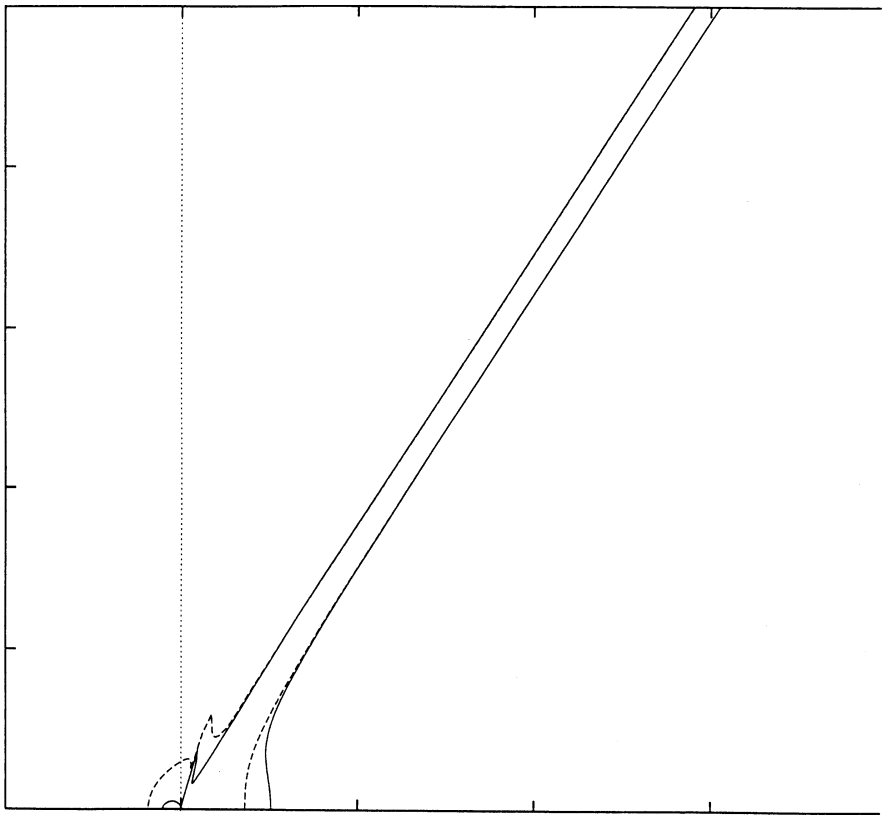


FIGURE 4. A typical directivity shape (for aluminium–water) for a vibrating semi-infinite strip with soft backing, the solid line is the result for the rigid strip (cf. Figure 3), and the dashed line is for the rigid strip coated with an acoustically soft material.

It is perhaps worthwhile considering the full matrix Wiener–Hopf problem that follows from the full boundary conditions; this is

$$\begin{pmatrix} \dfrac{\epsilon k_s^4 k_0 \gamma_d}{k_a \gamma_0} & -\dfrac{k_s^2 \gamma_d}{\mu} \\ \dfrac{\mu k_s^2 \epsilon k_0 R(\xi)}{k_a \gamma_0} & \dfrac{\epsilon k_2^4 k_0 \gamma_d}{k_a \gamma_0} \end{pmatrix} \begin{pmatrix} U_-(\xi) \\ T_-(\xi) - \dfrac{\mu R(\xi)}{\gamma_d k_s^2 i\xi_-} \end{pmatrix} = -\left(R(\xi) + \frac{\epsilon k_s^4 k_0 \gamma_d}{k_a \gamma_0} \right) \begin{pmatrix} U_+(\xi) \\ \sigma_+(\xi) \end{pmatrix}. \quad (4.6)$$

An approximate method of proceeding is to solve (4.6) by keeping leading order terms; this leads initially to two separate scalar functional equations that are (3.9) and, after using $T_-(\xi)$ deduced from (3.9) and some rearrangement, an equation identical to (4.2). The function $U_-(\xi)$ that is deduced is the same as that found in (4.2) – the asymptotic method advocated here is an intuitive physical interpretation of this factorization.

5 An incident Rayleigh wave

For a fluid/solid interface the unattenuated interfacial wave is a Stoneley wave (often called the Schölte wave) that has a wave speed, in the light fluid loading limit, close to that of the compressional wave speed of the fluid. In addition, there is a leaky Rayleigh wave that, in

https://doi.org/10.1017/S0956792597003239 Published online by Cambridge University Press

this light fluid-loading limit, is a perturbation of the usual Rayleigh wave that would propagate unattenuated along an elastic/vacuum interface. To first order in ϵ the exponential behaviour of the leaky wave in the fluid for $x > 0$ travelling to infinity is

$$\exp\left(i(k_r x-(k_0^2-k_r^2)^{\frac{1}{2}}y)-\frac{k_r(k_r^2-k_d^2)^{\frac{1}{2}}}{k_d\, d(k_0^2-k_r^2)^{\frac{1}{2}}}\epsilon k_0\left(x+\frac{k_r y}{(k_0^2-k_r^2)^{\frac{1}{2}}}\right)\right),$$

where d is defined as, Tew (1992a),

$$d=\frac{2}{k_s^4}\left((k_s^4-4k_r^4)+2k_r^4\left(\frac{(k_r^2-k_d^2)^{\frac{1}{2}}}{(k_r^2-k_s^2)^{\frac{1}{2}}}+\frac{(k_r^2-k_s^2)^{\frac{1}{2}}}{(k_r^2-k_d^2)^{\frac{1}{2}}}\right)\right), \tag{5.1}$$

which shows that the wave propagates into the fluid along an angle $\cos^{-1}(k_r/k_0)$ with respect to the x axis into the fluid. In practice, the distances involved, and $\epsilon \ll 1$, mean that a defect on the surface is often struck by what is in effect a Rayleigh wave. Unfortunately, the natural mathematical problem of a model defect diffracting an incident leaky Rayleigh wave from infinity is awkward to formulate due to the exponential decay of that wave along the surface. This is overcome by using the approach outlined here whereby the fluid and solid responses are separated. As noted by a referee, one could treat the incident leaky Rayleigh wave exactly; however, the wave could then have infinite amplitude at infinity and infinite power associated with it. Thus it is, perhaps, simpler and more direct to adopt the uncoupling procedure advocated here.

For brevity, a Rayleigh wave is taken to be incident from infinity upon a semi-infinite rigid strip lying along the interface $y = 0$ for $x < 0$; as in previous sections, the strip is in lubricated contact with the solid. This allows the functions (3.8) to be introduced and some analysis from §3 to be used directly.

First, consider a Rayleigh wave travelling to the left along the surface of a traction free elastic half space. Choosing the elastodynamic potentials in (2.2) as

$$\phi^{inc}(x,y)=\frac{4U\gamma_s(k_r)k_r^2}{(2k_r^2-k_s^2)k_s^2}\mathrm{e}^{-ik_r x-\gamma_d(k_r)y},\quad \psi^{inc}(x,y)=\frac{2Uk_r^2}{ik_r k_s^2}\mathrm{e}^{-ik_r x-\gamma_s(k_r)y}, \tag{5.2}$$

gives an incident Rayleigh wave that has $u_2(x,0) = U\mathrm{e}^{-ik_r x}$. Using the separation of the fluid and solid problems proposed here, the fluid sees a plane interface with a non-zero surface displacement applied and this generates a potential $\chi^{inc}(x,y)$ in the fluid that is

$$\chi^{inc}(x,y)=-\frac{i\omega U}{\gamma_0(k_r)}\mathrm{e}^{-ik_r x+\gamma_0(k_r)y}. \tag{5.3}$$

This represents an undamped surface wave travelling in the fluid with wave speed equal to the Rayleigh wave. It is important to note that an exact analysis leads to a free surface wave travelling at the Schölte wave speed, and does not explicitly identify this Rayleigh wave that is the undamped part of the leaky Rayleigh wave. The wave described above is used as our incident wave and is subtracted from the boundary value problem. Hence, for each field variable $f^{total}(x,y) = f^s(x,y)+f^{inc}(x,y)$, the superscript s is used to denote the scattered field, and this is now considered in detail.

Initially the elastic solid is considered in isolation with $y = 0, x > 0$ traction free, and $y = 0, x < 0$ with boundary conditions $\sigma_{12}^s(x,0) = 0$, $u_s^2(x,0) = -U\mathrm{e}^{-ik_r x}$. Using half-range

https://doi.org/10.1017/S0956792597003239 Published online by Cambridge University Press

transforms as discussed near (3.9), and as in Fredricks & Knopoff (1960), leads to an expression for $U^s_+(\xi)$, that is,

$$U^s_+(\xi) = \frac{U}{i(\xi - k_r)}\left(1 - \frac{(\xi+k_d)^{\frac{1}{2}} 2k_r\, S_+(k_r)}{(k_r+k_d)^{\frac{1}{2}}(\xi+k_r)\, S_+(\xi)}\right). \tag{5.4}$$

From the Fourier inverse, in the elastic solid there is a reflected Rayleigh wave and diffracted elastic body waves. However, the quantity of most interest here is the non-zero normal displacement along the interface for $x > 0$; this is represented by $U^s_+(\xi)$ in (5.4) and drives the fluid response. For the scattered waves the fluid initially sees a plane surface subject to a normal displacement that is $-U\mathrm{e}^{-ik_r x}$ for $x < 0$ and is represented by the inverse transform of $U^2_+(\xi)$ for $x > 0$. The fluid potential is deduced to be

$$\chi^s(x,y) = \frac{1}{2\pi}\int_\Gamma \frac{\omega U}{\gamma_0(\xi)} \frac{(\xi+k_d)^{\frac{1}{2}} 2k_r\, S_+(k_r)}{(k_r+k_d)^{\frac{1}{2}}(\xi^2 - k_r^2)\, S_+(\xi)} \mathrm{e}^{-i\xi x + \gamma_0(\xi) y}. \tag{5.5}$$

The pole at k_r gives a reflected Rayleigh wave contribution, that from the previous analysis gives the leading order behaviour of the leaky Rayleigh wave, and the pole at $-k_r$ recovers the loading on $x < 0$. Using the saddle approach gives a far field cylindrical wave in the fluid, that is,

$$\chi^s(r,\theta) \sim \frac{-i\omega U \mathrm{e}^{ik_0 r - \frac{i\pi}{4}}}{(2\pi k_0 r)^{\frac{1}{2}}} \frac{2k_r\, S_+(k_r)\,(k_d - k_0\cos\theta)^{\frac{1}{2}}}{(k_r^2 - k_0^2\cos^2\theta)\, S_-(k_0\cos\theta)\,(k_r+k_d)^{\frac{1}{2}}}, \tag{5.6}$$

r and θ are polar coordinates centred upon the plate edge. Provided $k_r < k_0$, this gives intense beam formation along both $\theta = \pi - \cos^{-1}(k_r/k_0)$ and $\theta = \cos^{-1}(k_r/k_0)$.

This is in contrast to the field produced by an incident Schölte wave upon the semi-infinite rigid strip, say $u_2^{inc}(x,0) = U\mathrm{e}^{-ik_{sch}x}$, that generates reflected surface waves, diffracted waves within the elastic solid, etc., together with a far field cylindrical wave in the fluid, that is,

$$\chi^s(r,\theta) \sim \frac{-i\omega U \mathrm{e}^{ik_0 r - \frac{i\pi}{4}}}{(2\pi k_0 r)^{\frac{1}{2}}} \frac{2k_{sch}\, L_+(k_{sch})\,(k_d - k_0\cos\theta)^{\frac{1}{2}}}{(k_{sch}^2 - k_0^2\cos^2\theta)\, L_-(k_0\cos\theta)\,(k_{sch}+k_d)^{\frac{1}{2}}}. \tag{5.7}$$

The intense beam formation is now both along an angle $\theta \sim \pi - \epsilon$, that is, in the direction of propagation of the surface wave and along the Rayleigh angle $\cos^{-1} k_r/k_0$. The former is demonstrated by using the factorization, valid in the neighbourhood of k_0, of $L_-(\xi)$ as

$$L_-(\xi) \sim \frac{(\xi - k_r)\, S_-(\xi)}{(\xi - k_{sch})}\left(1 + \frac{\epsilon k_s^4 k_0^{\frac{1}{2}}(k_0^2 - k_d^2)^{\frac{1}{2}}}{2^{\frac{1}{2}} k_d\, R(k_0)\,(\xi - k_0)^{\frac{1}{2}}}\right), \tag{5.8}$$

together with the asymptotic representation of k_{sch} for small ϵ, that is,

$$k_{sch} \sim k_0(1 + \tfrac{1}{2}u^2\epsilon^2), \tag{5.9}$$

where u is defined as

$$u = -k_s^4 \frac{(k_0^2 - k_d^2)^{\frac{1}{2}}}{k_d\, R(k_0)}. \tag{5.10}$$

The factorization contains a term that cancels any major contribution along $\theta \sim \epsilon$. The beam formation along $\theta \sim \pi - \epsilon$ is the analogue of that found by Crighton (1985) for the scattering of an incident surface wave by a fluid loaded elastic plate/rigid strip intersection;

https://doi.org/10.1017/S0956792597003239 Published online by Cambridge University Press

it occurs as for this surface wave the wavespeed is close to that of the compressional fluid waves, and most of the energy is contained within the fluid. The wave energy then continues past the edge to form the beam. The beam formation along the Rayleigh angle that occurs for ϵ small is generated by the reflected leaky Rayleigh wave. These far field directivities will be of value in a geometric ray theory approach to a more practical situation where, say, a plane wave is incident upon a finite length slit between two rigid plates, then both leaky Rayleigh and Schölte surface waves will be generated by the diffraction at each edge. These waves will then propagate to the other edge, and their subsequent diffraction will generate distinctive beams. Although it is important to note that the leaky Rayleigh wave has exponential decay along the surface, so the length scale of the strip, and ϵ, must be small for it to have any substantial effect.

6 Scattering by subsurface cracks

The previous examples have all been somewhat idealised; the aim of demonstrating that this separation into fluid and solid pieces is a valid approach is to allow us to tackle somewhat harder problems in this light fluid loading-limit.

In a recent paper, Craster (1997) solves scattering problems involving incident plane, or interfacial, waves and a subsurface crack of arbitrary orientation. This is done using numerical techniques applied to a system of coupled integro-differential equations, and the results are checked using reciprocity relations and power flow theorems devised for fluid–solid scattering problems. The purpose of this section is to tackle the same problems, but instead of solving the integro-differential equations using the full Green's function, the separation into fluid and solid pieces is adopted. Thus, one solves the elastic scattering problem in the absence of the fluid, the Green's functions utilised take a simpler form and the numerics are simpler, the resulting solution is then used to drive the response in the fluid. The elastic scattering problems have been treated by several authors, for instance Achenbach *et al*. (1983) or Van der Hijden & Neerhoff (1984); the treatment here follows the latter authors.

If we consider plane waves upon a subsurface crack, the coordinate system and geometry is as shown in figures 5 and 6 (note the coordinate axes are now altered from that adopted in previous sections), the boundary conditions $\sigma_{13} = \sigma_{33} = 0$ on $x_3 = 0$, $|x_1| < a$, that is, the crack is stress free, then one can utilise the reciprocal theorem to show that the scattered field at a point (p_1, p_2) within the fluid or solid is given by

$$u_k^{sc}(p_1, p_3) = \int_{-a}^{a} \sigma^G_{i3;k}(x_1, 0; p_1, p_3)\,[u_i^{sc}(x_1, 0)]\,\mathrm{d}x_1. \tag{6.1}$$

The summation convection is adopted over repeated suffices, the superscript *sc* denotes scattered fields, and $[u_i]$ denotes the unknown jump in displacement across the crack faces – the aim of any numerical method is to find this. Once the jump in displacement is found, Eq. (6.1) gives the scattered fields. The stress tensor $\sigma^G_{ij;k}$ is the Green's state associated with

$$\sigma^G_{kj,j}(\mathbf{x}; \mathbf{p}) + \rho\omega^2 u^G_k(\mathbf{x}; \mathbf{p}) = -\delta(\mathbf{x} - \mathbf{p}). \tag{6.2}$$

The approximation utilised here will be to use the Green's function found in the absence of the fluid for all numerical work. This is not as complicated as that involving fluid coupling, and when we evaluate the scattered field in the fluid using steepest descents to

https://doi.org/10.1017/S0956792597003239 Published online by Cambridge University Press

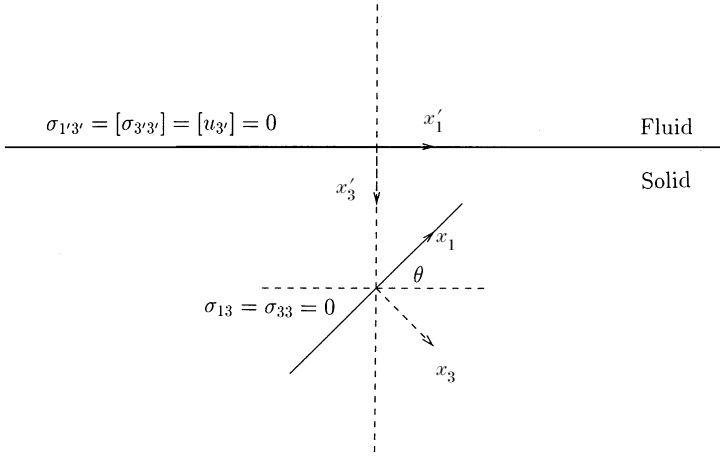


FIGURE 5. The coordinate systems associated with the subsurface crack.

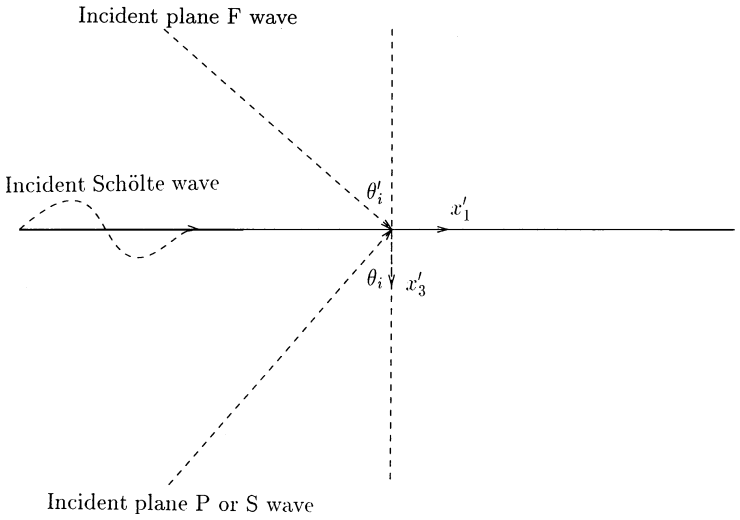


FIGURE 6. The incident wave fields.

identify the directivity the correct Green's function incorporating fluid effects is used, this Green's function is given in Craster (1997) as a Fourier integral. This later step is analytic; the bulk of the numerical effort is in programming in the kernel functions, thus demonstrating that one can utilise the simpler Green's functions is of value. Moreover, many numerical solutions exist for other defect-wave interactions beneath interfaces so these could be similarly utilised.

The terms $[u_i(x_1, 0)]$ are written as $\Psi_i(x_1)$ and the following integro-differential equation is deduced:

$$-\sigma_{i3}^{in}(p_1, 0) = \lambda\delta_{i3}\frac{\partial}{\partial p_k}\int_{-a}^{a}\sigma_{j3;k}^{G}\,\Psi_j\,\mathrm{d}x_1 + \mu\frac{\partial}{\partial p_3}\int_{-a}^{a}\sigma_{j3;i}^{G}\,\Psi_j\,\mathrm{d}x_1 + \mu\frac{\partial}{\partial p_i}\int_{-a}^{a}\sigma_{j3;3}^{G}\,\Psi_j\,\mathrm{d}x_1, \quad (6.3)$$

that relates the incident stress upon the crack faces to the unknown jump in displacement across the crack faces. The equation (6.3) holds for $i = 1, 3$, and as $p_3 \to 0$ for $|x_1| < a$, the

https://doi.org/10.1017/S0956792597003239 Published online by Cambridge University Press

superscript *in* denotes incident fields. The argument for the stresses is $(x_1, 0; p_1, p_3)$ and of Ψ is (x_1). These integro-differential equations are treated by expanding the unknowns as a sequence of Chebyshev polynomials, that is,

$$\Psi_\alpha(x_1) = \frac{4}{i} \sum_{n=1}^{\infty} a_{\alpha;n}\, \psi_n(x_1), \quad \text{where} \quad \psi_n(x_1) = \begin{cases} \cos(n \arcsin(x_1/a)) & n \text{ odd} \\ i \sin(n \arcsin(x_1/a)) & n \text{ even}, \end{cases} \tag{6.4}$$

for $\alpha = 1, 3$, where the $a_{\alpha;n}$ are to be determined. These are the natural eigenfunctions and incorporate the correct edge behaviour.

Both sides of (6.3) are multiplied by the complex conjugate of a term of (6.4); complex conjugates are denoted by an overbar, and integrated over the crack faces. All the integrations over the crack faces are done analytically using

$$\int_{-a}^{a} \bar{\psi}_m(x_1)\, \mathrm{e}^{ikx_1}\, \mathrm{d}x_1 = \frac{\pi m}{k} J_m(ka) \tag{6.5}$$

and related integrals; the $J_m(ka)$ are Bessel's functions of the first kind. This sequence of operations yields the set of simultaneous equations

$$b_{i;m} = \sum_{n=1}^{\infty} K_{ij;mn}\, a_{j;n}, \quad m = 1, 2, 3, \ldots \tag{6.6}$$

and $i = 1, 3$. The kernel functions $K_{ij;mn}$ are given as integrals involving Bessel functions (see Van der Hijden & Neerhoff, 1984). The left-hand side is known in terms of the incident field as

$$b_{i;m} = \frac{-1}{\mu\pi} \int_{-a}^{a} \sigma_{i3}^{in}(x_1, 0)\, \bar{\psi}_m(x_1)\, \mathrm{d}x_1 \quad \text{for } i = 1, 3. \tag{6.7}$$

Thus, after some numerical work, and after truncating the infinite sum at N such that the relative difference between variables is less than a specified tolerance, the $a_{j;n}$ are identified. Thus the jump in displacement is determined, and hence the scattered fields everywhere are effectively known.

Within the fluid the far-field for $k_0 r \gg 1/e^2$ is

$$u_\alpha^{rad}(r, \hat{\mathbf{x}}') = \frac{i}{4} \left(\frac{2}{\pi k_0 r} \right)^{\frac{1}{2}} \exp(ik_0 r - i\pi/4)\, G_F(\phi)\, \hat{\mathbf{x}}'_\alpha, \tag{6.8}$$

where $x_1' = -r \sin\phi$, $x_3' = -r\cos\phi$ and $\hat{\mathbf{x}}'$ is the unit vector in the $\mathbf{x}'$ direction, and $-\pi/2 \leqslant \phi \leqslant \pi/2$. The function $G_F(\phi)$ is given explicitly in Craster (1997). In the following figures the directivity gains $\bar{G}_F(\phi)$ are plotted, where:

$$\bar{G}_F(\phi) = \frac{\omega \lambda_f}{16\pi [P_{body}]} |G_F(\phi)|^2. \tag{6.9}$$

The proportion of the total time average power converted to body waves within the elastic solid is $[P_{body}]$.

To demonstrate the accuracy of the proposed scheme, let us consider a subsurface parallel crack and an incident plane elastic P wave along $\theta_i = \pi/3$ with $k_s a = 3$, $d/a = 0.5$

https://doi.org/10.1017/S0956792597003239 Published online by Cambridge University Press

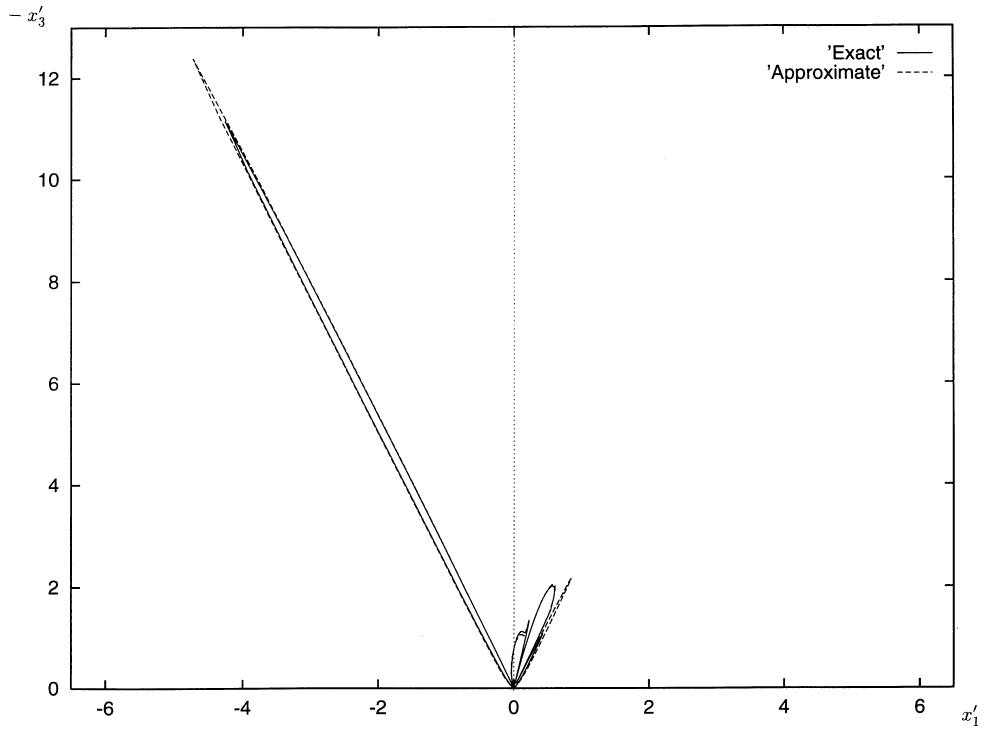


FIGURE 7. The directivity gains within the fluid for an incident P wave along $\theta_i = \pi/3$, $k_s = 3$, $d/a = 0.5$, $\epsilon = 0.08$. Exact solution (solid line), approximate (dashed).

and $\epsilon = 0.08$; the material parameters are $k_d = \frac{1}{2}k_s$ and $k_0 = 3k_s$. The scattered field within the fluid is shown in Figure 7; the solid line is the exact solution using the full Green's function, and the dashed line is the approximate solution; they are virtually indistinguishable.

The beam formation is along the Rayleigh angles, and we note that the beam in one direction is much larger than the other. In fact, the beam along the Rayleigh angle in $x_1' > 0$ is about the same magnitude as those due to head wave contributions. This can be rationalized using the solution found in the absence of the fluid. With no fluid coupling the fraction of scattered power converted to Rayleigh waves propagating in the $-x_1'$ direction is 7% versus that in the $+x_1'$ direction of only 0.7%; with light fluid loading the beam formation is, in part, due to this power being redirected along the Rayleigh angles.

As discussed in previous sections, the situation of a leaky Rayleigh wave incident from infinity is not particularly convenient to consider, but the uncoupling scheme can be utilised to generate solutions. In Figure 8 the scattered field within the fluid for an incident Rayleigh wave upon a parallel crack, with the same material parameters as in the previous figure taken, is shown. The beam formation is now particularly evident. As before, in the absence of the fluid the power converted to Rayleigh waves gives an indication of the magnitude of the peaks; 50% is converted to Rayleigh waves propagating in the $+x_1'$ direction versus 10% in the $-x_1'$ direction.

https://doi.org/10.1017/S0956792597003239 Published online by Cambridge University Press

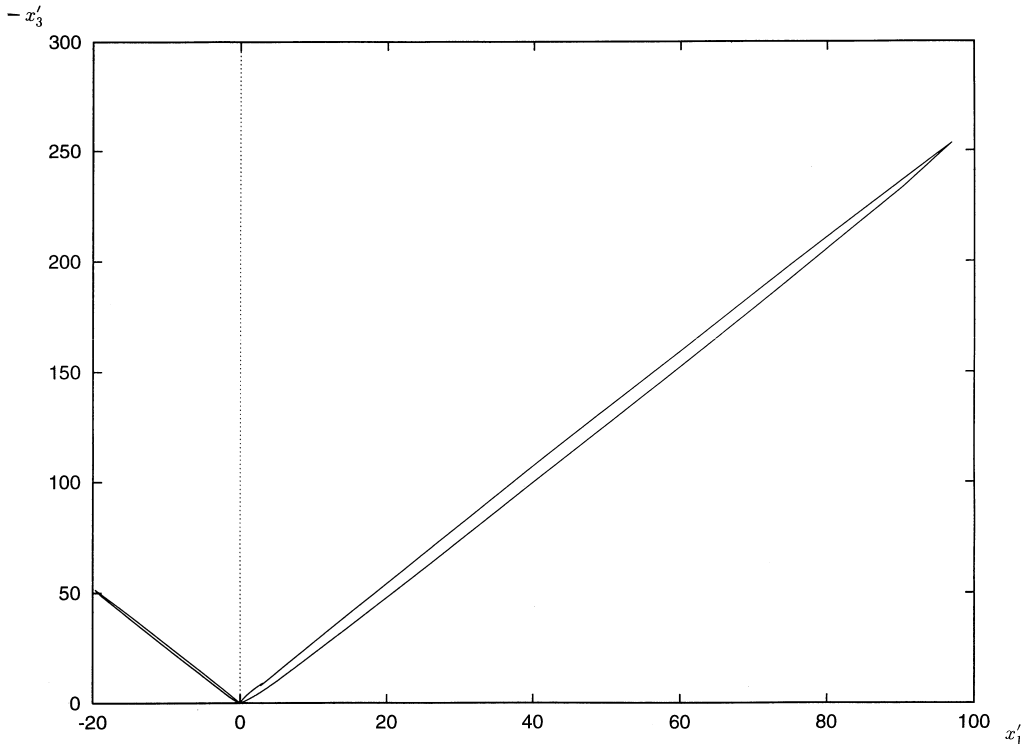


FIGURE 8. The directivity gains within the fluid for an incident Rayleigh wave with $k_s a = 3$, $d/a = 0.5$, $\epsilon = 0.08$.

7 Conclusion

A procedure is described whereby elastodynamic solutions involving an elastic half-space bounded above by a vacuum are generalized to include the effect of weak fluid coupling. This enables a simplified interpretation to be made for the body wave generated in the fluid; to leading order it is forced by the elastic response, and this allows problems previously out of reach to be tackled in this limit. The far-field directivity associated with the cylindrical wave in the fluid is explicitly identified.

There is an inherent non-uniformity associated with leaky surface waves. The non-uniform behaviour occurs along critical angles within the fluid for $1 \ll k_0 r \ll 1/\epsilon^2$; the method presented here correctly detects the presence of transition regions in the neighbourhood of the Rayleigh angle. In addition, a simple matching scheme determines the leading order amplitude of the interfacial Schölte waves.

The methods described in this paper allow one to take any time harmonic problem involving defects upon a plane traction free elastic half space and generalise those results to involve light fluid loading. Similar methods can be used for defects within the solid, or for line sources in the fluid, although the details are slightly different and will be dealt with elsewhere. Transient problems involving acoustic pulses are also amenable to this perturbation approach (Craster, 1996b).

The importance of this approach apart from the specific examples treated here is the breadth of further applications, for instance there are currently few problems solved

https://doi.org/10.1017/S0956792597003239 Published online by Cambridge University Press

involving fluid/anisotropic elastic interactions, or fluid/layered elastic media interactions: the underlying idea here carries across directly. Similarly scattering by defects upon curved fluid/solid interfaces, circular elastic cylinders and in three dimensions have a simplified interpretation in this light fluid loading limit.

A referee has pointed out that the approach utilised here will need to be significantly modified if several defects are upon the interface. Resonance effects due to diffracted Schölte, or leaky Rayleigh waves, may occur. In the related fluid-elastic plate situations, Leppington (1976) demonstrates how to overcome these difficulties and it may be that a similar approach will be of value in the fluid-elastic solid cases.

Acknowledgements

It is a pleasure to thank Dr R. H. Tew for several helpful conversations and the referees for their useful comments and additional references.

Financial support by the EPSRC via an advanced fellowship is gratefully acknowledged. In addition the author is grateful for a grant from the Nuffield Foundation under the Awards for Newly Appointed Lecturers Scheme that has been of considerable assistance.

Appendix A

Consider the function $L(\xi)$, defined as

$$L(\xi) = \frac{(2\xi^2 - k_s^2)^2 - 4\xi^2(\xi^2 - k_s^2)^{\frac{1}{2}}(\xi^2 - k_d^2)^{\frac{1}{2}} + \epsilon k_s^4 k_0 (\xi^2 - k_d^2)^{\frac{1}{2}}/k_d(\xi^2 - k_0^2)^{\frac{1}{2}}}{2(k_d^2 - k_s^2)(\xi^2 - k_{sch}^2)}, \tag{A1}$$

where k_{sch} is the positive real root of the numerator. If $\epsilon = 0$ this function reverts to one involving the usual Rayleigh function with k_r replacing k_{sch}, and this function is denoted by $S(\xi)$ in the text. $L(\xi)$ is split into the product of two functions analytic in the upper and lower complex ξ planes, i.e. $L(\xi) = L_+(\xi)\, L_-(\xi)$ using Cauchy's theorem from which $L_-(\xi)$ is determined explicitly as

$$\log L_-(\xi) = -\frac{1}{\pi}\left(\int_{k_d}^{k_s} \tan^{-1}\phi_1 \frac{\mathrm{d}\tau}{\tau - \xi} + \int_{k_2}^{k_0} \tan^{-1}\phi_2 \frac{\mathrm{d}\tau}{\tau - \xi}\right), \tag{A2}$$

where the branch of the inverse tangent is chosen so that $0 \leqslant \tan^{-1}\phi \leqslant \pi$. The functions ϕ_1 and ϕ_2 are

$$\phi_1 = \frac{4\tau^2(\tau^2 - k_d^2)^{\frac{1}{2}}(k_s^2 - \tau^2)^{\frac{1}{2}} + \epsilon k_s^4 k_0 (\tau^2 - k_d^2)^{\frac{1}{2}}/k_d(k_0^2\tau^2)^{\frac{1}{2}}}{(2\tau^2 - k_s^2)^2}, \tag{A3}$$

$$\phi_2 = \frac{\epsilon k_s^4 k_0 (\tau^2 - k_d^2)^{\frac{1}{2}}}{k_d(k_0^2 - \tau^2)^{\frac{1}{2}}((2\tau^2 - k_s^2)^2 - 4\tau^2(\tau^2 - k_d^2)^{\frac{1}{2}}(\tau^2 - k_s^2)^{\frac{1}{2}})}, \tag{A4}$$

and $L_+(\xi) = L_-(-\xi)$. A similar function is treated by Freund & Achenbach (1967). In the limit as $\epsilon \to 0$ then $L_-(\xi)$ tends to

$$\log L_-(\xi) \sim -\frac{1}{\pi}\int_{k_d}^{k_s} \tan^{-1}\left(\frac{4\tau^2(\tau^2 - k_d^2)^{\frac{1}{2}}(k_s^2 - \tau^2)^{\frac{1}{2}}}{(2\tau^2 - k_s^2)^2}\right)\frac{\mathrm{d}\tau}{\tau - \xi} - \log\frac{(\xi - k_0)}{(\xi - k_r)}, \tag{A5}$$

the second term occurs because of the choice of branch cut for the inverse tangent; the first term is $\log S_-(\xi)$. This implies that $(\xi - k_{sch})\, L_-(\xi) \sim (\xi - k_r)\, S_-(\xi)$ as $\epsilon \to 0$, as we would

https://doi.org/10.1017/S0956792597003239 Published online by Cambridge University Press

expect (this uses $k_{sch} \sim k_0 + O(\epsilon^2)$ as $\epsilon \to 0$). A more general asymptotic factorisation, valid in the neighbourhood of k_0 is given in (5.8). The following asymptotic properties of $L_+(\xi)$ are useful, in the limit as $|\xi| \to \infty$ then $L_+(\xi) \to 1$, and $L_+(0) = k_s^2(1+\epsilon)^{\frac{1}{2}}/k_{sch}(2(k_s^2 - k_d^2))^{\frac{1}{2}}$. The roots $\pm k_{sch}$ are found explicitly; for the positive real root k_{sch} is

$$k_{sch} = k_s^2 \left(\frac{1+\epsilon}{2(k_s^2 - k_d^2)} \right)^{\frac{1}{2}} \exp\left(\frac{1}{2\pi} \int_{k_d}^{k_s} \tan^{-1} \phi_1 \frac{2\mathrm{d}\tau}{\tau} + \frac{1}{2\pi} \int_{k_s}^{k_0} \tan^{-1} \phi_2 \frac{2\mathrm{d}\tau}{\tau} \right). \tag{A6}$$

References

Abrahams, I. D. (1986) Scattering of sound by a semi-infinite elastic plate with a soft backing; a matrix Wiener–Hopf problem. *IMA J. Appl. Maths.* **37**, 227–245.

Achenbach, J. D. (1973). *Wave Propagation in Elastic Solids.* North-Holland, Amsterdam.

Achenbach, J. D., Lin, W. & Keer, L. M. (1983) Surface waves due to scattering by a near-surface parallel crack. *IEEE Trans. Son. Ultrason.* **30**, 270–276.

Barbone, P. E. (1995) Approximate diffraction coefficients by the method of matched asymptotic expansions. *Wave Motion* **22**, 1–16.

Craster, R. V. (1996a) A canonical problem for fluid–solid interfacial wave coupling. *Proc. Roy. Soc. Lond. A* **452**, 1695–1711.

Craster, R. V. (1996b) Wavefront expansions for pulse scattering by a surface inhomogeneity. *Quart. J. Mech. Appl. Math.* **49**, 657–674.

Craster, R. V. (1997) Scattering by cracks beneath fluid–solid interfaces. *J. Sound Vibration.* To appear.

Crighton, D. G. (1972). Acoustic edge scattering of elastic surface waves. *J. Sound Vib.* **22**, 25–32.

Crighton, D. G. (1985). Acoustics of a stiff locally reacting structure. *Proc. Roy. Soc. Lond. A* **397**, 99–120.

Crighton, D. G. (1989) The 1989 Rayleigh Medal Lecture: fluid loading – the interaction between sound and vibration. *J. Sound Vib.* **133**, 1–27.

Crighton, D. G. & Innes, D. (1984) The modes, resonances and forced response of elastic structures under heavy fluid loading. *Phil. Trans. R. Soc. Lond. A* **312**, 295–341.

Fredricks, R. W. & Knopoff, L. (1960) The reflection of Rayleigh waves by a high impedance obstacle on a half space. *Geophysics* **25**, 1195–1202.

Freund, L. B. & Achenbach, J. D. (1967) Diffraction of a plane pulse by a semi-infinite barrier at a fluid-solid interface. *J. Appl. Mech.* **34**, 571–578.

Heckl, M. (1962) Vibrations of point driven cylindrical shells. *J. Acoust. Soc. Am.* **34**, 1553–1557.

Leppington, F. G. (1976) Scattering of sound waves by finite membranes and plates near resonance. *Quart. J. Mech. Appl. Math.* **29**, 527–546.

Maidanik, G. (1967) Acoustic radiation for a driven, coated infinite plate backed by a parallel infinite baffle. *J. Acoustic Soc. Am.* **42**, 32–35.

Rawlins, A. D. (1975) The solution of a mixed boundary value problem in the theory of diffraction by a semi-infinite plane. *Proc. Roy. Soc. Lond. A* **346**, 469–484.

Tew, R. H. (1992*a*) Diffraction of sound by a surface inhomogeneity at a fluid-solid interface. *Euro. J. Appl. Math.* **3**, 115–145.

Tew, R. H. (1992b) Non-specular reflection phenomena at a fluid-solid boundary. *Proc. Roy. Soc. Lond. A* **437**, 433–449.

Van Der Hijden, J. H. M. T. & Neerhoff, F. L. (1984a) Diffraction of elastic waves by a sub-surface crack (in-plane motion). *J. Acoust. Soc. Am.* **75**, 1694–1704.

https://doi.org/10.1017/S0956792597003239 Published online by Cambridge University Press